



Trans. Nonferrous Met. Soc. China 32(2022) 1781-1794

Transactions of Nonferrous Metals Society of China

www.tnmsc.cn



Design and preparation of Al-Fe-Ce ternary aluminum alloys with high thermal conductivity

Gan LUO^{1,2}, Xiong ZHOU¹, Cheng-bo LI^{1,3}, Jun DU¹, Zheng-hua HUANG²

- 1. School of Materials Science and Engineering, South China University of Technology, Guangzhou 510640, China;
- 2. Guangdong-Hong Kong Joint Research and Development Center on Advanced Manufacturing Technology for Light Alloys, Institute of New Materials, Guangdong Academy of Sciences, Guangzhou 510650, China;
 - 3. School of Materials and Environment, Guangxi University for Nationalities, Nanning 530006, China

Received 26 May 2021; accepted 25 March 2022

Abstract: Ce element was introduced to modify Al–2%Fe (mass fraction) binary alloy. The microstructures, crystallization behavior, electrical/thermal conductivities and mechanical properties of these alloys were systematically investigated. The results indicated that the appropriate Ce addition decreased the recalescence temperature and growth temperature of Al–Fe eutectic structure, improved the morphology and distribution of Fe-containing phase, and simultaneously increased the conductivity and mechanical properties. The annealed treatment improved the thermal conductivity of these alloys due to the decreasing concentration of point defects. Rolling process further broke up the coarser Fe-containing phases into finer particles and made the secondary phases uniformly distributed in the $\alpha(Al)$ matrix. After subsequent annealing treatment and rolling deformation, the thermal conductivity, ultimate tensile strength and hardness of the Al–2%Fe–0.3%Ce (mass fraction) alloy reached 226 W/(m·K), (182±1.4) MPa and HBW (49.5±1.7), respectively.

Key words: Al-Fe-Ce alloys; Ce modification; thermal conductivity; mechanical properties

1 Introduction

The rapid development in the electronic communication industry has boosted the requirement of structure materials with high heat dissipation and lightweight [1–4]. Aluminum (Al) alloys have been paid considerable attention owing to their excellent castability, high specific strength and good electrical/thermal conductivity (ETC) [5,6]. Previous studies have demonstrated that thermal conductivity and mechanical properties are contradictory factors in aluminum alloys [6–8]. The reasonable design of alloy composition is the key issue to prepare novel Al alloy with high ETC

and acceptable mechanical properties. It has been reported that solute atoms and intermetallic compounds have the most obvious influence on the ETC of Al alloys at ambient temperature [9–11]. Moreover, solute atoms can reduce the thermal conductivity to a greater extent than intermetallic compounds [10]. Thus, Fe element with low solid solubility in the α (Al) matrix can be acted as the main alloying element for preparing high thermal conductivity Al alloys [8,12]. Considering the castability in industrial production, a near-eutectic Al–2wt.%Fe alloy was set as the research object in this study.

Rare earth elements like La, Ce and Yb, play a positive role in conducting aluminum alloys,

because they can refine grain size of $\alpha(Al)$ [13,14], modify intermetallic compounds [15,16] and meliorate the distribution of the inclusion phases [17]. Such effects of Ce addition on aluminum alloys have been widely reported. LI et al [17] showed that adding (0.05-0.16) wt.% Ce into Al rod can simultaneously improve electrical conductivity and tensile strength owing to reducing the solid solubility of impurity and refining the $\alpha(Al)$ grains. KANG et al [18] found that combined addition of Ce and Mg improves the strength and ductility of Al-7Si-0.3Mg-0.2Fe alloy, which is mainly attributed to the grain refinement, eutectic Si modification and Fe-containing intermetallic compound refinement. In a study conducted by ZHANG et al [19], they have compared the difference of La and Ce on the electrical conductivity of pure aluminum. Ce has a stronger purification ability of Fe and Si impurities in the $\alpha(Al)$ matrix than La, resulting in the formation of Al-Fe-Si-Ce compounds. As a result, the proper addition of Ce increases the electrical conductivity of as-cast pure Al from 62.3%(IACS) to 63.6%(IACS). Moreover, LIANG et al [20] analyzed the improvement mechanism of RE (consisting of both Ce and La) on the mechanical properties of Al-2wt.%Fe and concluded that RE are elements enriched in the front of the solid/liquid interface and Al₈Fe₂Ce is formed, thus refining $\alpha(Al)$ grains. The evidences reviewed here seem to suggest that the addition of Ce always plays a positive role in conducting aluminum alloys.

However, little is known from previous studies on the relationship between conductivity properties and microstructures of Al–2wt.%Fe with different Ce contents. The purpose of this study was to study the modification effect of Ce element on the microstructure of near-eutectic Al–2wt.%Fe alloy in the as-cast, annealed and rolled states and establish the relationship between solidification parameters and microstructure by cooling curve thermal analysis (CCTA). The modification behaviors of Ce element and specific modification mechanism were further discussed.

2 Experimental

2.1 Preparation of samples

Commercially pure aluminum (99.7 wt.% including ~0.12 wt.% Si and ~0.07 wt.% Fe),

Al-20wt.%Fe and Al-10wt.%Ce master alloys were used as raw materials. The pure aluminum ingots were melted in an electrical resistivity furnace at 1023 K. The Al-20wt.%Fe master alloy was then added to form the Al-2wt.%Fe alloy. The molten alloy was stirred with a MgO ceramic rod for approximately 1 min to ensure the uniformity of the melt. The Al-10wt.%Ce master alloy was added in different proportions to obtain Al-2%Fe-xCe (x=0, 0.1, 0.2, 0.3, 0.5, in wt.%, the same below) ternary alloy. When the temperature of molten alloy decreased to 993 K, the melts were poured into a steel mold (100 mm \times 45 mm \times 15 mm) preheated to 473 K.

The as-cast ingots were cut into three parts at 40 mm and 80 mm away from the right. The middle and right ones were subsequently homogenized at 773 K for 24 h, and then cooled inside the furnace to ambient temperature before rolling. The rolling process was carried out by a double-roller mill at room temperature. The right one was rolled to 3 mm with a total rolling deformation of 80%. The rolling process of the Al–2%Fe–xCe is schematically shown in Fig. 1.

2.2 Measurements

The microstructures of the as-cast, annealed and rolled alloys were observed using optical microscope (OM, Leica DMI 3000) and scanning electron microscope (SEM, Zeiss Gemini 300). The measuring software, Nano Measurer 1.2, was adopted to measure the value of secondary dendrite arm spacing (SDAS). Energy dispersive spectrum (EDS, Oxford X-MaxN) was conducted to determine the second phase composition. Phase constitution was analyzed by X-ray diffraction system (XRD, Bruker D8 Advance) with Cu K_{α} radiation. Tensile tests were measured using an AG-X100kN testing machine with a strain rate of 1 mm/min at room temperature. Besides, hardness measurements were performed using an HB-3000 hardness tester at a load of 62.5 kg. Three samples for each group were used to obtain the mechanical properties of each state alloy.

The thermal diffusivities of the alloys with sizes of $d12.7 \text{ mm} \times 3 \text{ mm}$ in the round disk were determined by the flash method (Netzsch LFA457). The densities of samples were determined by the Archimedes method (DH-300). The specific heat capacities of the alloys were calculated using

the Neumann–Kopp rule. Thus, the thermal conductivity (λ) is calculated using the following relation:

$$\lambda = \alpha \rho c_p$$
 (1)

where α is the thermal diffusivity (mm²/s), ρ is the density (g/cm³), and c_p is the specific heat capacity (J/(g·K)). The uncertainty for the thermal conductivity was estimated to be less than 5%. Each test was repeated three times for each sample, and the average value was taken to ensure the reliability of the experiment. Moreover, to determine the contribution of free electrons in the heat transferring processing, electrical conductivity measurement was conducted on the samples by the vortex method (FD-101) [7].

The CCTA was conducted to investigate

relationship between crystallization microstructure by using the double thermocouple method [21–23]. One of the K-type thermocouples was located closely to the wall, and the other was situated in the center of melts. The position of the thermocouples was set at 20 mm from the bottom of the crucible where the top and bottom were insulated to control radial heat flow shown in Fig. 2. The temperature—time data were recorded continuously by using the NI 9212 Series high-speed data acquisition system, which had a data collection rate of 80 points/s. The acquisition system was connected to the laptop, installed with LabVIEW 2015. The thermal analysis was carried out at least three times to ensure the repeatability of the experimental results.

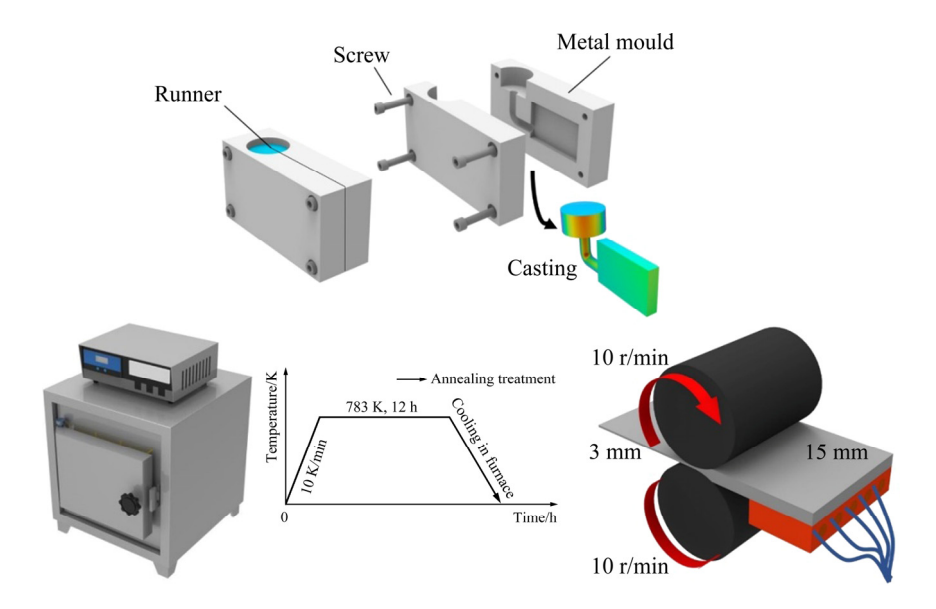


Fig. 1 Schematic diagram of preparation and corresponding measurements of Al-2%Fe-xCe alloys

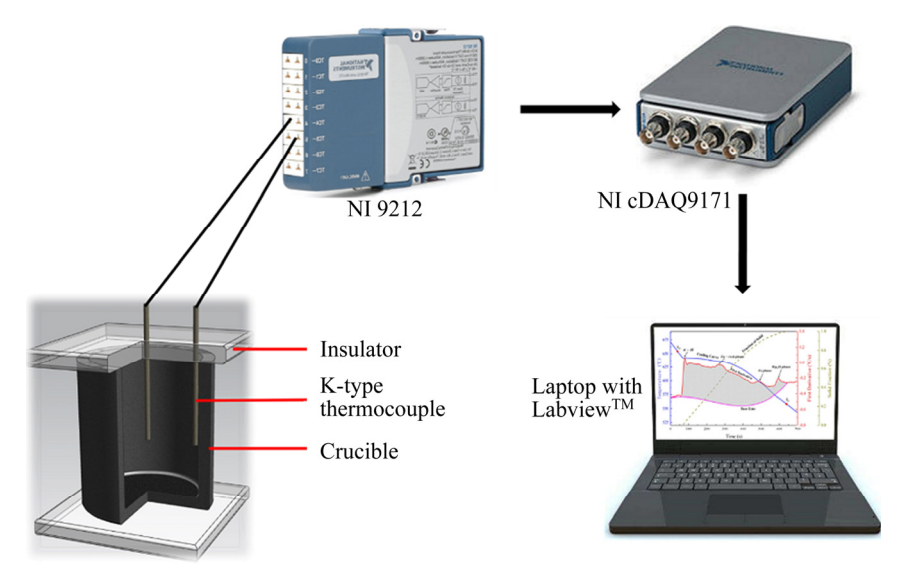


Fig. 2 Schematic diagram of CCTA using double-thermocouple method

3 Results and discussion

3.1 Effect of Ce addition on microstructure of Al-2%Fe alloy

Figure 3 presents microstructures of as-cast Al–2%Fe alloys with different Ce contents. It can be obviously observed that the microstructures of Al–2%Fe alloy (Fig. 3(a)) consist of long needle-like primary Al–Fe phase, primary α (Al) phase and eutectic structure (α (Al) + Al₃Fe). The modification of Ce element has an obvious influence on the α (Al) grain and Fe-containing phase. The statistical results of the SDAS are summarized in Fig. 4. These data show that the SDAS value firstly decreases from 13.1 to 8.9 μ m with the Ce content increasing from 0 to 0.3%. When the Ce content exceeds 0.3% and reaches

0.5%, this value increases to 11.9 μ m. The results obtained by statistical analysis confirm that the optimal microstructure appears in the Al-2%Fe-0.3%Ce alloy.

Moreover, the morphologies and distribution of Al–Fe phases have been changed by Ce modification. The long needle-like primary Al–Fe phase (Point *A* of Fig. 5(a)) is prominently transformed into fine particles. According to the results of SEM–EDS shown in Figs. 5(b) and (c), the fine particles have two forms. One is the claw-like Al–Fe–Ce ternary intermetallic compound (Point *C* of Fig. 5(b)) with the size of ~1 μm. The other is the short rod-like Al–Fe–Ce phase (Point *D* of Fig. 5(c)) with the length of ~2 μm. The molar ratio of Fe to Ce for both claw-like and rob-like Al–Fe–Ce compound is close to 2:1. Combined with the experimental results of

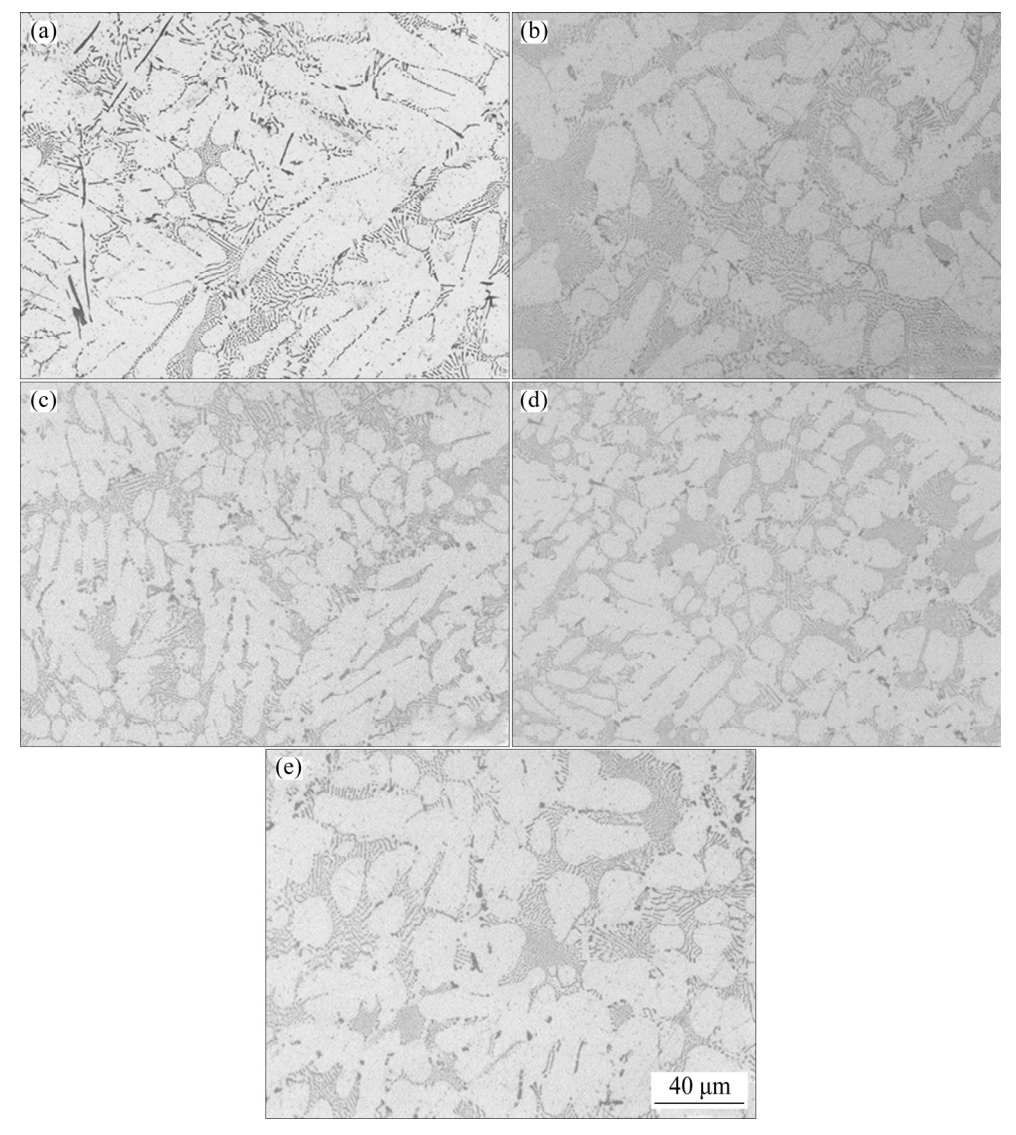


Fig. 3 Microstructures of as-cast Al-2%Fe-xCe alloys: (a) x=0%; (b) x=0.1%; (c) x=0.2%; (d) x=0.3%; (e) x=0.5%

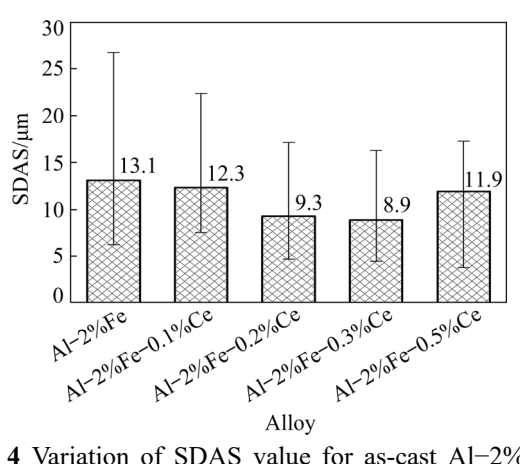


Fig. 4 Variation of SDAS value for as-cast Al-2%Fe-xCe alloy

XRD, the Al-Fe-Ce compound could be thought to Al₁₀Fe₂Ce. While the Ce content increases to 0.5%, nanoscale particles (Point E of Fig. 5(d)) were found in the α (Al) matrix and could be the Al-Ce phase. As for the eutectic Al-Fe phase, the continuous network of eutectic structure was broken down and changed to more dispersed and divorced morphology shown in Fig. 3.

Through the homogeneous annealing treatment, the primary Al–Fe phases were decomposed into short rods and fine particles, as presented in Fig. 6(a). No significant differences were found in the Ce-modified Al–2%Fe alloys after annealing treatment (Figs. 6(b–e)). Furthermore, the

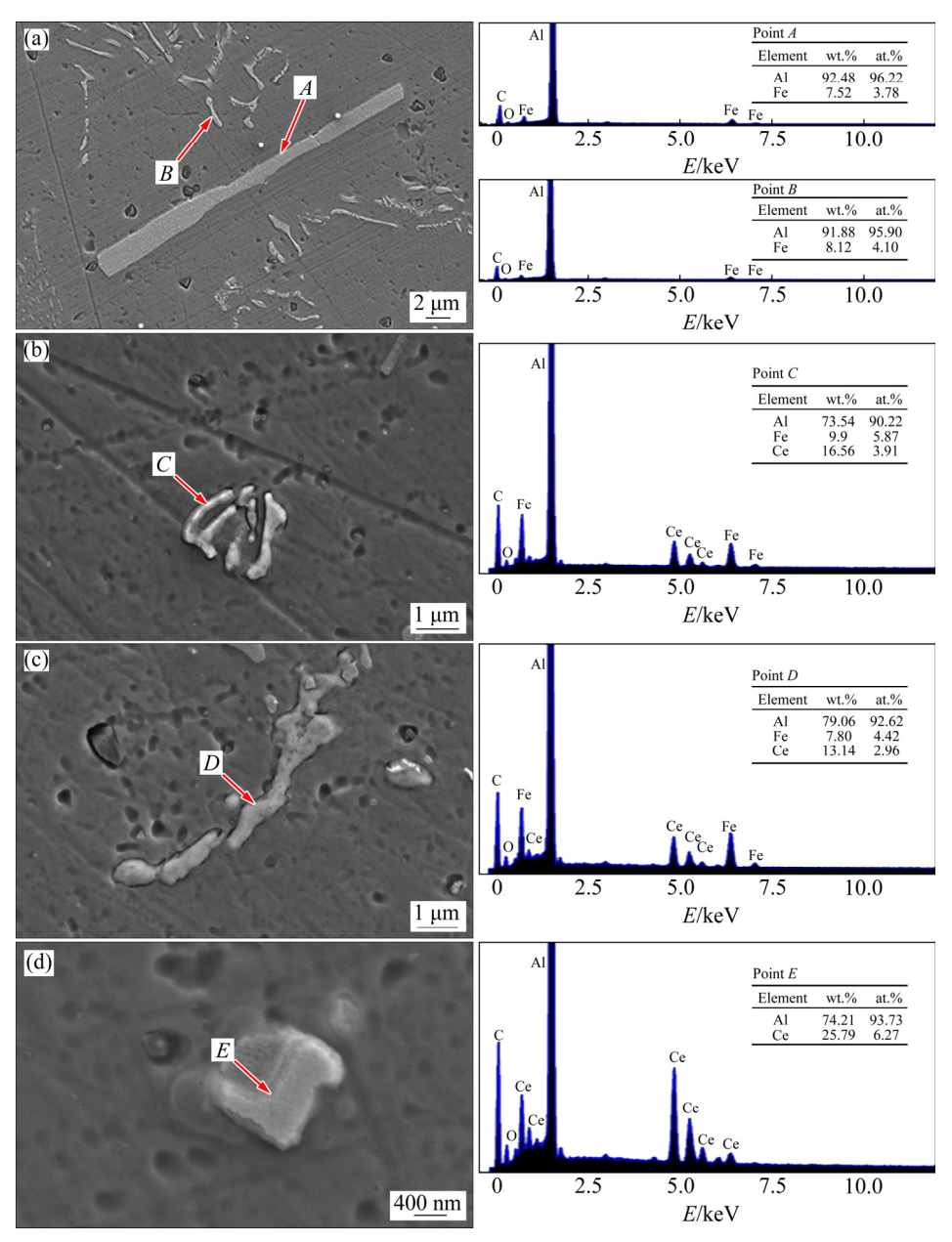


Fig. 5 SEM images of as-cast Al-2%Fe (a), Al-2%Fe-0.3%Ce (b), and Al-2%Fe-0.5%Ce (c, d) alloys, and corresponding EDS results

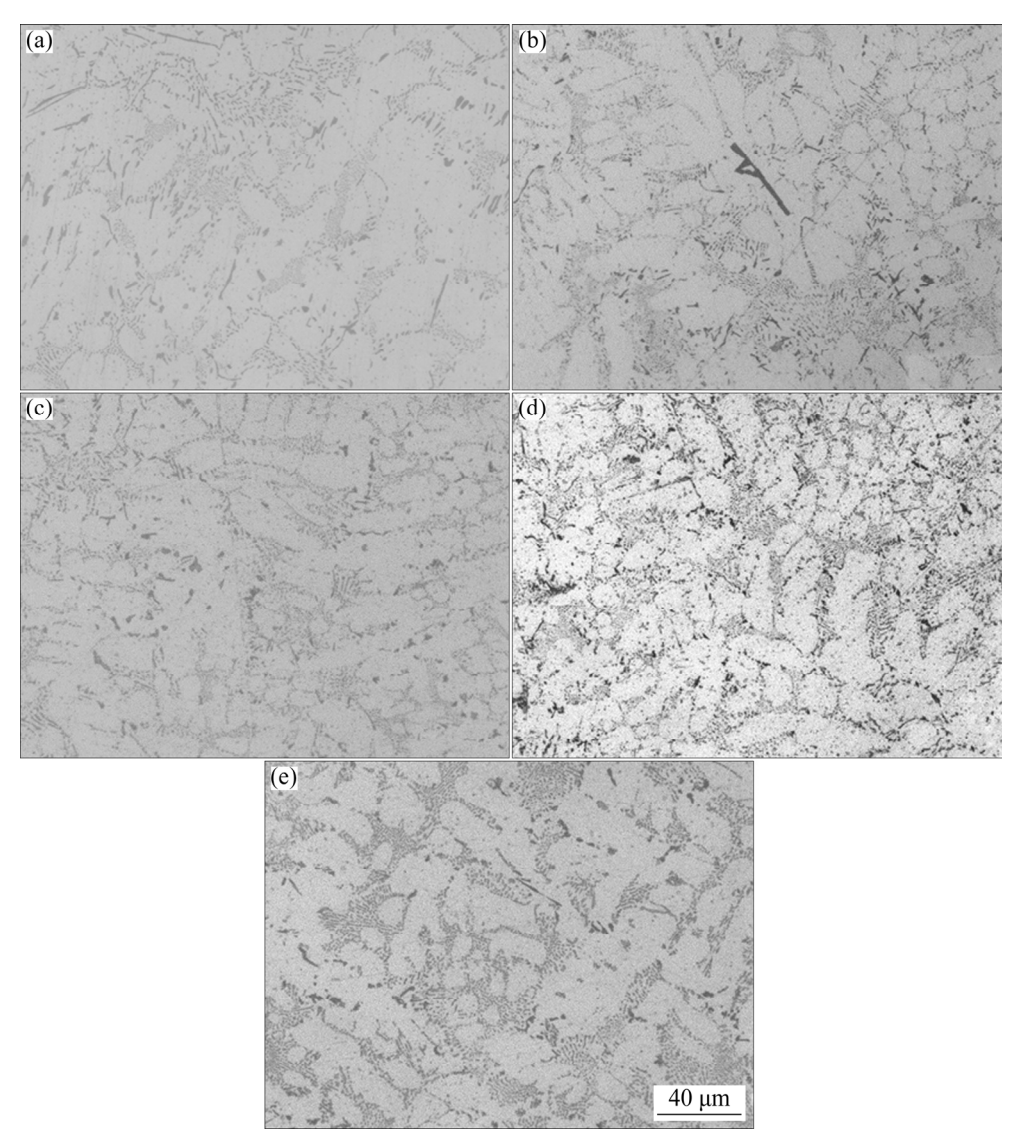


Fig. 6 Microstructures of homogeneously annealed Al–2%Fe–xCe alloys: (a) x=0%; (b) x=0.1%; (c) x=0.2%; (d) x=0.3%; (e) x=0.5%

subsequent rolling deformation made the secondary phases uniformly distributed in the $\alpha(Al)$ matrix, as provided in Fig. 7. It can be observed that the texture was formed in the rolled Al-2%Fe-xCe alloys.

The major metallurgical reactions can be identified by the solidification curve because the latent heat evolution release results in the creation of inflection points that change the slope of the curve. Figure 8 represents the cooling curves recorded during the solidification of the Al-2%Fe-xCe alloys with the corresponding first derivative and second derivative curves. The derivative cooling curves provide more details for each metallurgical reaction. Figure 8(b) shows a magnified plot of the α(Al) phase highlighting

information of phase evolution during solidification for the primary $\alpha(Al)$ phase. The related characteristic temperatures of Al-2%Fe alloys with different Ce contents are shown in Table 1. In Table 1, T_N is the temperature of initial nucleation, which is determined by the point at the intersection of the zero line and the second derivative curve when the d^2T/dt^2 (T is temperature and t is time) curve shifts upward. Moreover, the crest on the d^2T/dt^2 curve corresponds to zero point on the dT/dt curve which indicates the minimum temperature (T_{Min}) and the onset of latent heat release. The d^2T/dt^2 will go down and then up to the abscissa which corresponds to zero point on dT/dt curve, namely T_G . Once these characteristic points are determined on the derivative curve, they

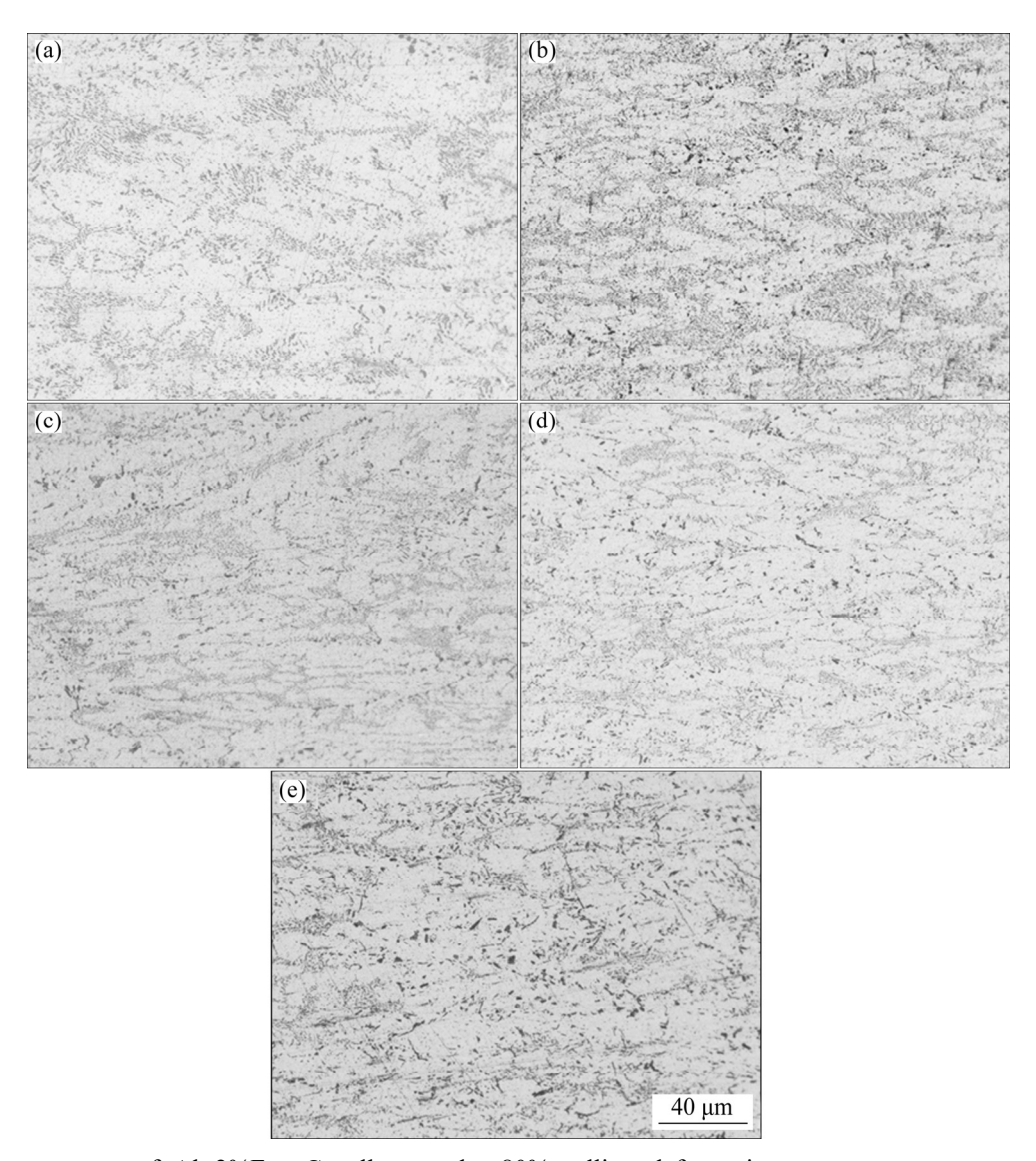


Fig. 7 Microstructures of Al–2%Fe–xCe alloys under 80% rolling deformation at room temperature: (a) x=0%; (b) x=0.1%; (c) x=0.2%; (d) x=0.3%; (e) x=0.5%

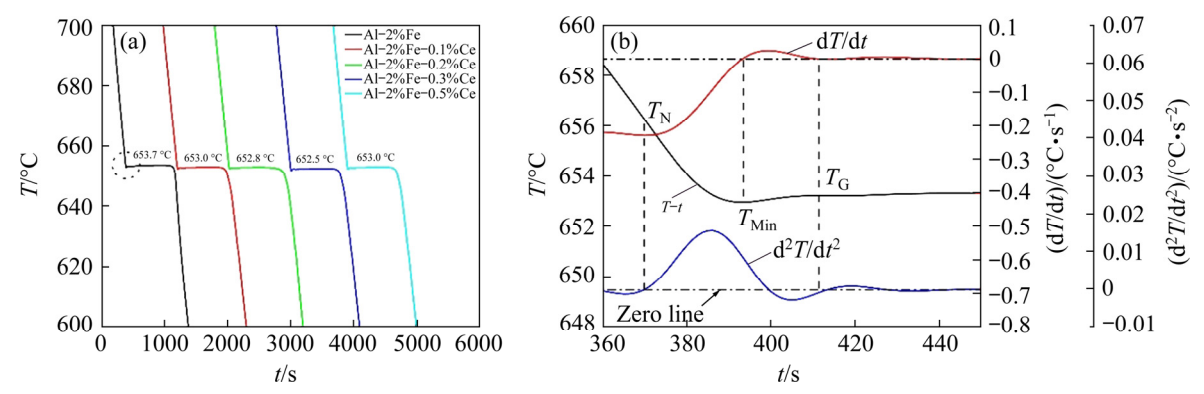


Fig. 8 Solidification curves of Al-2%Fe-xCe melts (a) and magnified plots for determining characteristic points T_N , T_G and T_{Min} (b)

are projected onto the original cooling curve, and the temperature value for each transformation is obtained. The recalescence temperature, $\Delta T_{\rm R}$, is the

eutectic difference value between $T_{\rm G}$ and $T_{\rm Min}$. $T_{\rm EG}$ is the growth temperature of Al–Fe eutectic structure, which is determined by the crystallization

platform on the original cooling curve. At the Al–Fe eutectic growth temperature, the latent heat of crystallization released during the solidification process compensates for the heat lost to the air. The corresponding characteristic temperatures are determined and listed in Table 1.

Table 1 Characteristic temperatures of Al–2%Fe–*x*Ce alloys containing different contents of Ce element

<i>x</i> /wt.%	T _N /°C	T _{Min} /°C	T _G /°C	T _{EG} /°C	$\Delta T_{\rm R}/^{\circ}{ m C}$
0	656.23	652.95	653.22	653.7	0.27
0.1	656.10	652.74	652.99	653.0	0.25
0.2	655.36	652.51	652.70	652.8	0.19
0.3	655.18	652.33	652.36	652.5	0.03
0.5	655.44	652.32	652.83	653.0	0.51

The cooling curves of Al–2%Fe eutectic alloys with different Ce contents are shown in Fig. 8(a). Different behaviors are observed during the solidification of these Ce-containing alloys as the Ce content increases. The experimental results show that the Al-Fe eutectic growth temperature, $T_{\rm EG}$, gradually decreases from 653.7 to 652.5 °C with the Ce content increasing from 0 to 0.3%. Then, $T_{\rm EG}$ increases to 653.0 °C when the Ce content reaches 0.5%. In the previous research in Refs. [21–23], $T_{\rm EG}$ has a close connection to the distribution and morphology of eutectic structure. In this study, the decreasing eutectic growth temperature inhibits the growth of Fe-containing phase, which obviously changes the morphology of Al₃Fe phases from long needles to fine particles (Figs. 3(a-d)).

Moreover, the characteristic temperatures of $\alpha(Al)$ phase are presented in Fig. 8(b) and Table 1. The initial nucleation temperature, T_N , stabilizes in the range from 655 to 657 °C. There is no inevitable connection between T_N and Ce content. It is worth mentioning that the minimum nucleation temperature, T_{Min} , gradually decreases from 652.95 to 652.32 °C as the Ce content increases from 0 to 0.5%. The recalescence temperatures of the samples are calculated and listed in Table 1. There is a significant positive correlation between ΔT_R and SDAS. The value of ΔT_R firstly declines from 0.27 to 0.03 °C with the Ce content increasing from 0 to 0.3%, and then increases to 0.51 °C when the Ce content reaches 0.5%. The variation of ΔT_R is similar to that of SDAS. Therefore, we will further

determine the relationship between ΔT_R and SDAS.

KURZ and FISHER [24] have put forward the criterion formula of SDAS under the condition of unsteady heat flow. The criterion formulae of SDAS can be written as presented in Eqs. (2) and (3):

$$\lambda_{\text{SDAS}} = K(Mt_{\text{f}})^{1/3} \tag{2}$$

$$\ln M = \frac{\Gamma D \ln(c_t^{\rm m} / c_0)}{m_{\rm L} (1 - k_0)(c_0 - c_t^{\rm m})}$$
(3)

where λ_{SDAS} is the value of SDAS, K is a constant which is related to alloy compositions, t_f is the time of local solidification, Γ is the Gibbs-Tomopson coefficient, D is the solute diffusion coefficient in the liquid phase, k_0 is the equilibrium partition coefficient, m_L is the slope of liquidus, and c_0 and $c_t^{\rm m}$ are the initial solute content of the melt and the solute content in the liquid phase, respectively. In this study, $t_{\rm f}$ could be considered as constant because of the same process parameters of casting. Thus, λ_{SDAS} is dependent on the value of M. According to Eq. (3), the M value is mainly determined by the alloy composition and solute diffusion coefficient. Combined with the Al-Ce binary phase diagram [12], the solid solution of Ce in $\alpha(Al)$ is limited due to the large difference between the atomic radii of Ce and Al. In the initial stage of crystallization, when the $\alpha(Al)$ phases grow, Ce atoms are extruded into the solid phase and enriched at the front of the solid/liquid interface, resulting in the solute redistribution and increasing the supercooling of components. The surface interface-enriched Ce atoms reduce the growth rate of $\alpha(Al)$ phase and decrease the value of SDAS.

It has been estimated that the recalescence phenomenon appears during the solidification process due to the heat release rate of phase transition being greater than the heat dissipation rate of metal. In our investigation, the decreasing recalescence temperature means that the heat release rate of phase transition becomes slower. In other words, the growth rate of $\alpha(Al)$ phase is reduced. Combined with the above analysis on the criterion formula of SDAS, we could infer that the decreasing recalescence temperature reduces the growth rate of $\alpha(Al)$ phase, decreases the value of SDAS and refines the $\alpha(Al)$ grains.

The growth temperature of Al–Fe eutectic structure, $T_{\rm EG}$, can be identified in Fig. 8 and Table 1. The most interesting aspect of the data is in the correlation between $T_{\rm EG}$ and morphology and

distribution of eutectic Al-Fe phase. Firstly, it can be observed that T_{EG} gradually decreases from 653.7 to 652.5 °C with the Ce content increasing from 0 to 0.3%, and then if the Ce content is higher than 0.3% and reaches 0.5%, T_{EG} will increase to 653.0 °C. Due to the low cooling rate during the CCTA, the eutectic temperature is close to the equilibrium crystallization temperature. According to the binary phase diagram of Al-Fe [12], the theoretical eutectic temperature of the Al-Fe binary alloy is 653 °C, which is in good agreement in our experimental results. To eliminate the interference of environmental factors, we suppose that the theoretical eutectic temperature of the Al-Fe binary alloy is 653.7 °C in this study. Thus, the actual supercooling degrees with 0.1%, 0.2%, 0.3% and 0.5% Ce additions are 0.7, 0.9, 1.2 and 0.7 °C, respectively. The eutectic temperature decreases by 1.2 °C with 0.3% Ce addition, which indicates that the eutectic reaction occurs at a greater degree of supercooling upon the addition of Ce.

For heterogeneous nucleation, the critical nucleation energy (ΔG) can be written as follows:

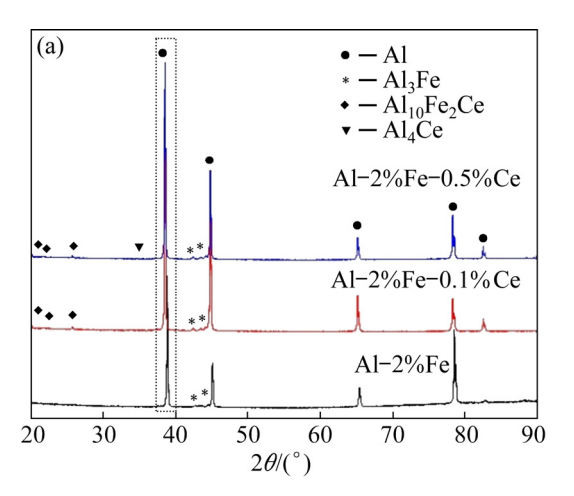
$$\Delta G = \frac{16\pi\gamma^3 T_{\rm m}^2}{3L_{\rm m}\Delta T} \cdot \frac{(2 - 3\cos\theta + \cos^3\theta)}{4} \tag{4}$$

where γ is the surface energy per unit area of the crystal embryo, $T_{\rm m}$ is the temperature of liquidus, $L_{\rm m}$ is the latent heat of crystallization, ΔT is the actual supercooling degree, and θ is the contact angle between the nucleus and base surface. Equation (4) demonstrates that the critical nucleation energy is related to the actual supercooling degree. The addition of Ce element increases the actual supercooling degree, decreases the critical nucleation energy and stimulates the nucleation of eutectic Al–Fe phases, which significantly improves the morphology and distribution of eutectic Al–Fe phase.

3.2 Effect of Ce addition on lattice parameters of $\alpha(AI)$

The XRD patterns of Al–2%Fe–xCe alloys are shown in Fig. 9. Figure 9(a) shows that the as-cast Al–2%Fe eutectic alloy consists of cubic α (Al) and monoclinic Al₃Fe (Al₁₃Fe₄). The addition of 0.1% Ce generates orthorhombic Al₁₀Fe₂Ce. For the as-cast Al–2%Fe–0.5%Ce alloy, a new phase, tetragonal Al₄Ce, is detected. The results of XRD patterns are in agreement with the Al–Fe–Ce

ternary phase diagram shown in Fig. 10. It can be seen from the results in Fig. 9(b) that when the Ce content of as-cast Al-2%Fe-xCe alloys increases from 0 to 0.1%, the 2θ value decreases significantly.



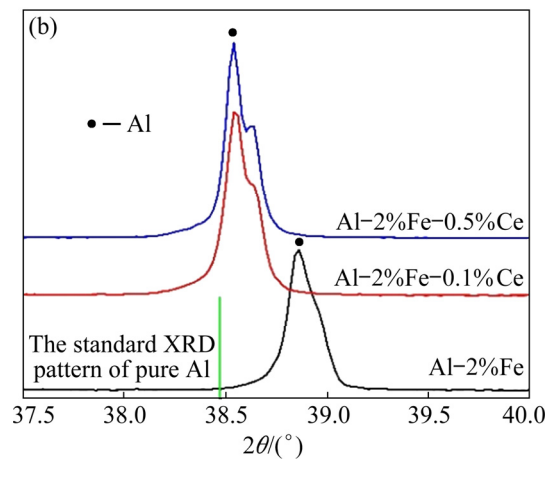


Fig. 9 XRD patterns (a) and partial enlarged details (b) of as-cast Al-2%Fe-xCe alloys

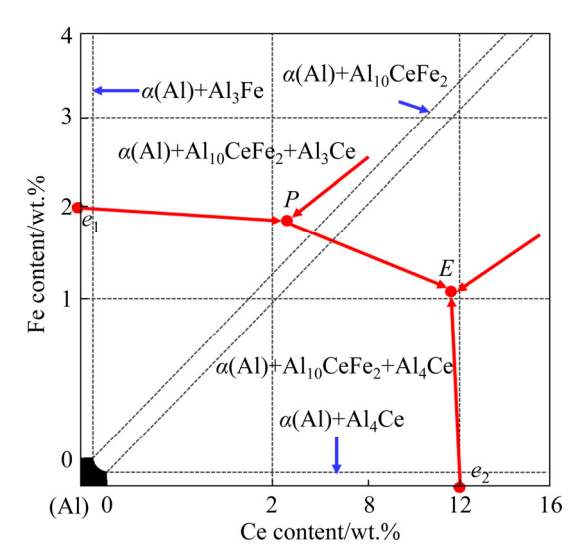


Fig. 10 Phase diagram of Al-Fe-Ce ternary alloy at Al-rich corner

Furthermore, the 2θ value hardly changes with the Ce content increasing to 0.5%.

According to the Bragg's formula [25,26], $2d\sin\theta = \lambda_1$ (d is the lattice distance, and λ_1 is the wavelength), the decrease of 2θ value indicates the increase of d value. It has been reported that the change of 2θ value is mainly attributed to the stress and solid solubility in the matrix [27]. Because the atom radius of Ce (0.183 nm) is larger than that of Al (0.143 nm), the solid solution of Ce atom will increase the value of d, resulting in a decrease of 2θ value [19]. Based on the Al-Ce and Al-Fe phase diagrams [12], the solid solubility values of Ce and Fe elements in $\alpha(Al)$ matrix are extremely low at room temperature. Moreover, Fe (radius of 0.127 nm) and Si (radius of 0.134 nm) are the inevitable impurities in aluminum alloys. Because of the non-equilibrium solidification in the casting process, the super-saturated solid solution will be formed, which consists of Fe, Si and Ce in the $\alpha(Al)$ matrix. As shown in Fig. 9(b), the 2θ value of Al-2%Fe-xCe alloys decreases and is close to that of standard pure aluminum (see the green line of

Fig. 9(b)) with the increase of Ce content. This appearance means that the contents of the solid solution atoms, Fe and Si, decrease. In other words, the Ce element has a strong purification ability of Fe and Si elements in the $\alpha(Al)$ matrix, causing the formation of Al₁₀Fe₂Ce phase (Fig. 10) and Al–Fe–Si–Ce compounds [19] rather than solid solution in the $\alpha(Al)$ matrix. In addition, it is worth noting that the 2θ value of Al–2%Fe–0.1%Ce alloy is the same as that of Al–2%Fe–0.5%Ce alloy. In other words, there is no much difference in the purification degree of these two alloys.

3.3 Effect of Ce addition on conductivity properties

Figure 11(a) provides the thermal diffusivity α of Al-2%Fe-xCe ternary alloys in different states. It can be observed that the thermal diffusivities of annealed and rolled samples are higher than that of as-cast ones under the same composition. The α value of as-cast Al-2%Fe eutectic alloy is only 84.09 mm²/s. When the Ce content is 0.1%, the thermal diffusivity reaches the highest value of

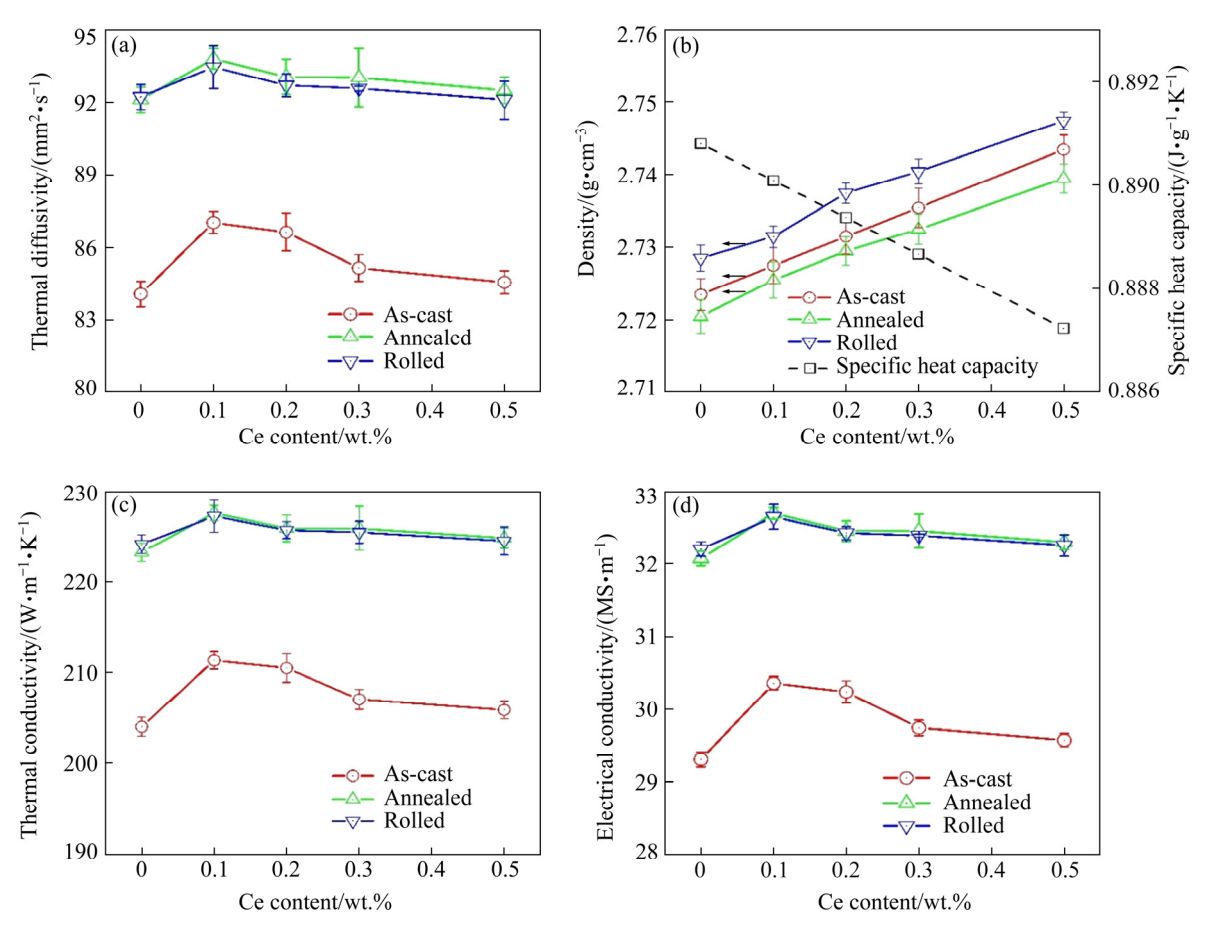


Fig. 11 Various properties of Al-2%Fe-xCe alloys in different states: (a) Thermal diffusivity; (b) Density and specific heat capacity; (c) Thermal conductivity; (d) Electrical conductivity

87.04 mm²/s, about 3.5% higher than that of Al–2%Fe alloy. However, the value of α decreases gradually with further increase of Ce content. While the Ce content reaches up to 0.5%, the thermal diffusivity decreases to 84.57 mm²/s. As shown in Fig. 11(b), the densities of different states for these alloys are in the following decreasing sequence: annealed alloy < as-cast alloy < rolled alloy. Moreover, the specific heat capacity, determined by Neumann–Kopp rule, decreases linearly with increasing Ce content.

The thermal conductivities of these alloys calculated by Eq. (1) are shown in Fig. 11(c). The variation of thermal conductivity is similar to that of thermal diffusivity. The highest thermal conductivity of the as-cast samples appears in Al-2%Fe-0.1%Ce with 211 W/(m·K). The most interesting result to emerge from the data is that the thermal conductivity of Al-2%Fe-0.1%Ce achieves to 228 W/(m·K) after annealing treatment and rolling process, which is approximately 11.8% higher than that of the as-cast Al-2%Fe alloys. In order to determine the contribution of free electrons in the heat transfer process, the measured results of electrical conductivity are provided in Fig. 11(d). There is a significantly positive correlation between thermal conductivity and electrical conductivity. For metal and alloys, the thermal conductivity is in proportion to the electrical conductivity according to the Wiedemann-Franz law as follows:

$$\lambda = LT\sigma$$
 (5)

where σ is electrical conductivity (MS/m), T is thermodynamic temperature (K) and L is the Lorentz number (L=2.44×10⁸ V⁻²·K⁻²). In this investigation, the ratio of thermal conductivity to electrical conductivity is about 6.96×10^{-6} V⁻²·K⁻¹. This means that the L value is equal to 2.34×10^{8} V⁻²·K⁻², which is in good agreement with our previous study on Al-2%Fe-xCo alloys [7].

In this study, Ce addition increases the conductivity properties of Al–2%Fe alloy, which may be explained by the purification of Ce element and the morphological improvement of Al–Fe phases. According to the experimental results of XRD shown in Fig. 9, the addition of Ce reduces the 2θ value and decreases the contents of Fe and Si atoms in the $\alpha(Al)$ matrix. This finding proves that adding 0.1% Ce could significantly reduce the degree of lattice distortion, thus the mean free path

of electrons increases, and the thermal conductivity of the alloy is improved. It has been widely recognized that the thermal conductivity of Al alloys is contributed by both the $\alpha(Al)$ matrix and the intermetallic compound. For the Ce-modified Al-2%Fe alloys, the continuous network of eutectic structure was broken down and changed to more dispersed and divorced morphology, indicates that Ce modification effectively reduces scattering of conducting electrons intermetallic compounds. This appearance is beneficial to the conductivity properties of alloys. However, two new phases, Al₁₀Fe₂Ce and Al₄Ce phases are found in the $\alpha(Al)$ matrix and act as the scattering sources, which are negative to the thermal conductivity. Thus, the conductivity properties of Ce-modified Al-2%Fe gradually decrease with the Ce content further increasing.

The ETC of annealed Al-2%Fe-xCe alloys is higher than that of as-cast alloys, which is owing to the elimination of point defect. It has been reported that vacancy is a strong scatter source, significantly decreasing the conductivity properties of aluminum alloys [28]. No significant differences are found between the ETC of annealed alloys and that of rolled alloys. This result may be explained by the two facts. One is that the increase of density is positive to the ETC. The other is that the rolling process refines the $\alpha(Al)$ grain and secondary phases, increasing the grain number and phase boundary, which decreases the ETC of Al-2%FexCe alloys. Therefore, there is no evident improvement of conductivity properties after the rolling process under the joint action of the above two factors.

3.4 Effect of Ce addition on mechanical properties

The mechanical properties of Al–2%Fe alloys with different Ce contents in different states are presented in Fig. 12. The results show that the tensile properties and hardness of the as-cast Ce-modified Al–2%Fe alloys are higher than that of the Ce-free alloy. This indicates that Ce modification is an effective method to improve the strength and plasticity of the near-eutectic Al–2%Fe alloy. The ultimate tensile strength, elongation and hardness of as-cast Al–2%Fe alloy are (102±1.5) MPa, (13.3±0.6)% and HBW (36.5±1.2),

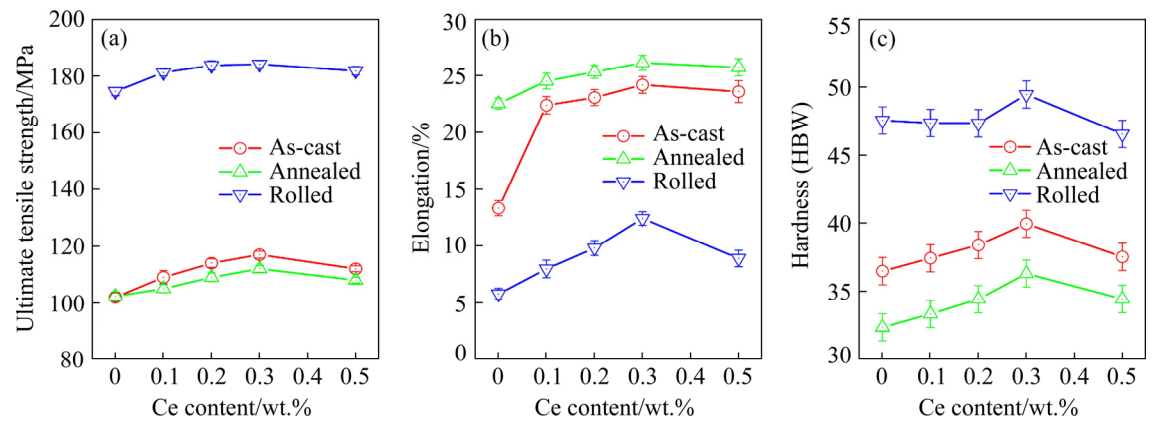


Fig. 12 Mechanical properties of Al-2%Fe-xCe alloys in different states: (a) Ultimate tensile strength; (b) Elongation; (c) Hardness

respectively. These performances gradually increase with the Ce content increasing. The optimal performances appear in the Al–2%Fe–0.3%Ce alloy with the ultimate tensile strength, elongation and hardness of (117±1.2) MPa, (24.2±0.8)% and HBW (40.0±1.5). Compared with the same properties of the as-cast Al–2%Fe alloy, these values show increments of about 15%, 82% and 10%, respectively. Further, the thermal conductivity of the as-rolled Al–2%Fe–0.3%Ce alloy is 226 W/(m·K), which is close to the optimum value of the Al–2%Fe–xCe alloy.

It is well known that the mechanical properties of Al-Fe alloys greatly depend on the size, morphology, and distribution of $\alpha(Al)$ and secondary phases. The SDAS value of $\alpha(Al)$ grain decreases from 13.1 to 8.9 µm as the Ce addition increases from 0 to 0.3%. The decreasing SDAS value is positive to the mechanical properties, especially the plasticity. Additionally, the addition of Ce element inhibits the formation of needleslike primary Al₃Fe phase and transforms it into claw-like Al₁₀Fe₂Ce phase. The Al₄Ce particle is an effective strengthening phase, which further improves the mechanical properties. According to Fig. 12(a), the homogeneous annealing treatment has little influence on the ultimate tensile strength of the Al-2%Fe-xCe ternary alloys. This heat treatment is beneficial to the plasticity of Al-2%Fe-xCe alloys. For example, the elongation of Al-2%Fe alloy increases from $(13.3\pm0.6)\%$ to $(22.5\pm0.5)\%$, which is the key to the subsequent deformation process.

Moreover, the ultimate tensile strength and hardness significantly increase through rolling deformation. The highest ultimate tensile strength and hardness are (182±1.4) MPa and HBW (49.5±1.7) for rolled Al-2%Fe-0.3%Ce alloy, which are about 56% and 24% higher than those of the as-cast Al-2%Fe-0.3%Ce alloy. The elongation of rolled samples inevitably decreases owing to the work hardening.

4 Conclusions

- (1) Ce modification decreases the SDAS value of $\alpha(Al)$ grain, transforms the long needle-like primary Al₃Fe phase into claw or rob-like Al₁₀Fe₂Ce phase and increases the divorced eutectic structures. The optimal microstructure can be achieved by adding 0.3% Ce.
- (2) The growth rate of $\alpha(Al)$ phase is reduced by adding Ce, resulting in the refinement of $\alpha(Al)$ grain. Moreover, the growth temperature of Al-Fe eutectic structure gradually decreases with the Ce content increasing. The morphology and distribution of eutectic Al-Fe phase are significantly improved.
- (3) Ce element has a strong purification of Fe and Si impurities in $\alpha(Al)$, resulting in the formation of Al–Fe–Ce and Al–Fe–Si–Ce intermetallic compounds rather than solid solution in the $\alpha(Al)$. Ce addition increases the ETC of Al–2%Fe alloy because of the purification in $\alpha(Al)$ and the morphological improvement of Al–Fe phases. The homogeneous annealing treatment and subsequent rolling deformation will significantly increase the conductivity properties of Al–2%Fe– α Ce alloys.
 - (4) The ultimate tensile strength and the

elongation of the Al-2%Fe-0.3%Ce alloy were (117±1.2) MPa and (24.2±0.8)%, respectively, about 15% and 82% higher than those of the matrix Al-2%Fe alloy. The improvement of mechanical properties was attributed to the refinement of SDAS and second phase strengthening. After subsequent annealing treatment and rolling deformation, the ultimate tensile strength and hardness of the Al-2%Fe-0.3%Ce alloy were achieved to be (182±1.4) MPa and HBW (49.5±1.7).

Acknowledgments

This work was financially supported by the National Natural Science Foundation of China (No. 52174363), the GDAS Project of Science and Technology Development, China (No. 2019GDASYL-0203002), the Key Research and Development Program of Guangdong Province, China (No. 2020B010186002), the Science and Technology Project of Zhaoqing City, China (Nos. 2021C003, 2018K006), and the Development Key **Technologies** for Material Microstructure Control of High Thermal Conductivity Casting Aluminum Alloy, China (No. 2014A030313221).

References

- [1] ARTHANARI S, JANG J C, SHIN K S. Corrosion performance of high pressure die-cast Al-6Si-3Ni and Al-6Si-3Ni-2Cu alloys in aqueous NaCl solution [J]. Transactions of Nonferrous Metals Society of China, 2018, 28: 2181-2189.
- [2] QI Ming-fan, KANG Yong-lin, LI Jing-yuan, SHANG Bei-yan. Improvement in mechanical, thermal conductivity and corrosion performances of a new high-thermally conductive Al–Si–Fe alloy through a novel R-HPDC process [J]. Journal of Materials Processing Technology, 2020, 279: 116586.
- [3] QI Ming-fan, KANG Yong-lin, XU Yu-zhao, WULABIEKE Z, LI Jing-yuan. A novel rheological high pressure diecasting process for preparing large thin-walled Al-Si-Fe-Mg-Sr alloy with high heat conductivity, high plasticity and medium strength [J]. Materials Science and Engineering A, 2020, 776: 139040.
- [4] WEN Cheng, GAN Jun-qi, LI Cheng-bo, HUANG Yu-jian, DU Jun. Comparative study on relationship between modification of Si phase and thermal conductivity of Al-7Si alloy modified by Sr/RE/B/Sb elements [J]. International Journal of Metalcasting, 2021, 15: 194-205.
- [5] HU Zhi, YAN Hong, RAO Yuan-sheng. Effects of samarium addition on microstructure and mechanical properties of as-cast Al-Si-Cu alloy [J]. Transactions of Nonferrous Metals Society of China, 2013, 23: 3228–3234.

- [6] JIANG Hong-xiang, LI Shi-xin, ZHENG Qiu-ju, ZHANG Li-li, HE Jie, SONG Yan, DENG Cong-kun, ZHAO Jiu-zhou. Effect of minor lanthanum on the microstructures, tensile and electrical properties of Al-Fe alloys [J]. Materials and Design, 2020, 195: 108991.
- [7] LUO Gan, HUANG Yu-jian, LI Cheng-bo, DU Jun. Microstructures and mechanical properties of Al–2Fe–xCo ternary alloys with high thermal conductivity [J]. Materials, 2020, 13: 3728.
- [8] ZHANG Xiao-yuan, ZHANG Hui, KONG Xiang-xin, FU Ding-fa. Microstructure and properties of Al-0.70Fe-0.24Cu alloy conductor prepared by horizontal continuous casting and subsequent continuous extrusion forming [J]. Transactions of Nonferrous Metals Society of China, 2015, 25: 1763-1769.
- [9] CHEN J K, HUNG H Y, WANG C F, TANG N K. Thermal and electrical conductivity in Al–Si/Cu/Fe/Mg binary and ternary Al alloys [J]. Journal of Materials Science, 2015, 50: 5630–5639.
- [10] SU C Y, LI D J, LUO A A, YING T, ZENG X Q. Effect of solute atoms and second phases on the thermal conductivity of Mg-RE alloys: a quantitative study [J]. Journal of Alloys and Compounds, 2018, 747: 431–437.
- [11] PAN Hu-cheng, PAN Fu-sheng, YANG Ru-min, PENG Jian, ZHAO Chao-yong, SHE Jia, GAO Zheng-yuan, TANG Ai-tao. Thermal and electrical conductivity of binary magnesium alloys [J]. Journal of Materials Science, 2014, 49: 3107–3124.
- [12] OKAMOTO H. Desk handbook: Phase diagrams for binary alloys [M]. New York: ASM International, 2010.
- [13] QIU Chuan-rong, MIAO Sai-nan, LI Xin-rong, XIA Xing-chuan, DING Jian, WANG Yong-ning, ZHAO Wei-min. Synergistic effect of Sr and La on the microstructure and mechanical properties of A356.2 alloy [J]. Materials and Design, 2017, 114: 563–571.
- [14] XIA Xing-chuan, ZHAO Qing-feng, PENG Yuan-yi, ZHANG Pan, CHEN Xue-guang. Precipitation behavior and mechanical performances of A356. 2 alloy treated by Al-Sr-La composite refinement-modification agent [J]. Journal of Alloys and Compounds, 2020, 818: 153370.
- [15] CHEN Yu, PAN Ye, LU Tao, TAO Shi-wen, WU Ji-li. Effects of combinative addition of lanthanum and boron on grain refinement of Al–Si casting alloys [J]. Materials and Design, 2014, 64: 423–426.
- [16] ZOU Yong-cheng, YAN Hong, YU Bao-biao, HU Zhi. Effect of rare earth Yb on microstructure and corrosion resistance of ADC12 aluminum alloy [J]. Intermetallics, 2019, 110: 106487.
- [17] LI Peng-fei, WU Zhi-gang, WANG Yun-li, GAO Xi-zhu, WANG Zai-yun, LI Zhi-qiang. Effect of cerium on mechanical performance and electrical conductivity of aluminum rod for electrical purpose [J]. Journal of Rare Earths, 2006, 24: 355–357.
- [18] KANG J, SU R, WU D Y, LIU C H, LI T, WANG L S, NARAYANASWAMY B. Synergistic effects of Ce and Mg on the microstructure and tensile properties of Al-7Si-0.3Mg-0.2Fe alloy [J]. Journal of Alloys and Compounds, 2019, 796: 267-278.

- [19] ZHANG Yu-liang, WEI Feng, MAO Jian, NIU Guo-dong. The difference of La and Ce as additives of electrical conductivity aluminum alloys [J]. Materials Characterization, 2019, 158: 109963.
- [20] LIANG Ya-hong, SHI Zhi-ming, LI Guo-wei, ZHANG Rui-ying, LI Ming. Effects of rare earth modification on microstructure refinement and mechanical properties of Al–2wt.%Fe alloys [J]. Materials Research Express, 2019, 6(10): 106504.
- [21] FARAHANY S, OURDJINI A, ABU BAKAR T A, IDRIS M H. A new approach to assess the effects of Sr and Bi interaction in ADC12 Al-Si die casting alloy [J]. Thermochimica Acta, 2014, 575: 179–187.
- [22] FARAHANY S, OURDJINI A, IDRSI M H, SHABESTARI S G. Evaluation of the effect of Bi, Sb, Sr and cooling condition on eutectic phases in an Al–Si–Cu alloy (ADC12) by in situ thermal analysis [J]. Thermochimica Acta, 2013, 559: 59–68.
- [23] FARAHANY S, IDRIS M H, OURDJINI A, FARIS F, GHANDVAR H. Evaluation of the effect of grain refiners on

- the solidification characteristics of an Sr-modified ADC12 die-casting alloy by cooling curve thermal analysis [J]. Journal of Thermal Analysis and Calorimetry, 2015, 119(3): 1593–1601.
- [24] KURZ W, FISHER D J. Fundamentals of solidification [M]. Zürich: Trans Tech Publications, 1992.
- [25] POPE, CHRISTOPHER G. X-ray diffraction and the Bragg equation [J]. Journal of Chemical Education, 1997, 74: 129–131.
- [26] CHEN S J, HOWITT D G, HARKER A B. A dynamical Bragg equation for high-order Laue zone reflections [J]. Scanning, 2000, 22: 156–160.
- [27] YU Yu-cheng, TANG Sha-wei, WANG Zhen-ling, HU Jin. Effects of coating contents on the interfacial reaction and tensile properties of Al₂O₃ coated-Al₁₈B₄O₃₃w/Al-Mg matrix composites [J]. Materials Characterization, 2015, 107: 327–333.
- [28] TAN Rui. Preparation and study of properties of moderate strength and high conductivity aluminum alloy wire [D]. Zhengzhou: Zhengzhou University, 2017. (in Chinese)

高导热性 AI-Fe-Ce 三元铝合金的设计与制备

罗干1,2,周雄1,李乘波1,3,杜军1,黄正华2

- 1. 华南理工大学 材料科学与工程学院,广州 510640;
- 2. 广东省科学院 新材料研究所 粤港轻合金先进制造技术联合研发中心,广州 510650;
 - 3. 广西民族大学 材料与环境学院, 南宁 530006

摘 要:采用 Ce 元素对 Al-2%Fe(质量分数)合金进行改性,并系统研究该合金的显微组织、凝固行为、电/热导率及力学性能。结果表明,添加适量 Ce 元素降低 Al-Fe 合金的再辉温度和共晶生长温度,改善含 Fe 相的形貌和分布,并同步提高该合金的热导率和力学性能。退火处理提高合金热导率主要归因于点缺陷浓度的降低。此外,轧制过程进一步将较粗的含 Fe 相分解成细小颗粒,使二次相均匀分布于 α (Al)基体。经过后续的退火和轧制处理,Al-2%Fe-0.3%Ce(质量分数)合金的热导率、抗拉强度和硬度分别达到 226 W/(m·K)、(182±1.4) MPa 和 HBW (49.5±1.7)。

关键词: Al-Fe-Ce 合金; Ce 改性; 导热性; 力学性能

(Edited by Wei-ping CHEN)